Radiative pion capture in ^{2}H, ^{3}He, and ^{3}H

J. Golak, R. Skibiński, K. Topolnicki, H. Witała, and A. Grassi
M. Smoluchowski Institute of Physics, Jagiellonian University, PL-30348 Kraków, Poland

H. Kamada
Department of Physics, Faculty of Engineering, Kyushu Institute of Technology, Kitakyushu 804-8550, Japan

A. Nogga
Institute for Advanced Simulation, Institut für Kernphysik, Jülich Center for Hadron Physics, and JARA - High Performance Computing, Forschungszentrum Jülich, D-52425 Jülich, Germany

L. E. Marcucci
Department of Physics, University of Pisa, IT-56127 Pisa, Italy
and INFN-Pisa, IT-56127 Pisa, Italy

(Received 23 July 2018; published 5 November 2018)

The $\pi^- + {}^2\mathrm{H} \to \gamma + n + n$, $\pi^- + {}^3\mathrm{He} \to \gamma + {}^3\mathrm{H}$, $\pi^- + {}^3\mathrm{He} \to \gamma + n + d$, $\pi^- + {}^3\mathrm{He} \to \gamma + n + n + p$, and $\pi^- + {}^3\mathrm{H} \to \gamma + n + n + n$ capture reactions are studied with the AV18 two-nucleon potential and the Urbana IX three-nucleon potential. We provide for the first time realistic predictions for the differential and total capture rates for all these processes, treating consistently the initial and final nuclear states. Our results are based on the single-nucleon Kroll-Ruderman-type transition operator and concentrate on the full treatment of the nuclear final state interactions. They are compared with older theoretical predictions and experimental data.

DOI: 10.1103/PhysRevC.98.054001

I. INTRODUCTION

Studies of radiative pion capture were initiated in 1951 by Panofsky, Aamodt, and Hadley [1], who measured the ratio of mesonic ($\pi^- + p \to n + \pi^0$) to radiative ($\pi^- + p \to n + \gamma$) capture of stopped negative pions in hydrogen. Measurements of capture reactions in the early 1950s played an important role in fixing fundamental properties of the pions and their interactions with the nucleons. Later, experiments performed at the Lawrence Radiation Laboratory in Berkeley delivered photon spectra from radiative pion capture on different nuclei. Many such measurements with improved resolution were conducted in the 1970s at the Swiss Institute for Nuclear Research (SIN) [later the Paul Scherrer Institute (PSI)] by a collaboration including the Universities of Lausanne, Munich, and Zurich. All the early experimental and theoretical work prior to January 1976 was summarized in Ref. [2]. Since we restrict ourselves to reactions with two and three nucleons in the present paper, we only refer the reader to Refs. [3–12] for later studies of systems with $A > 3$.

The studies of the $\pi^- + {}^2\mathrm{H} \to \gamma + n + n$ reaction concentrated on the extraction of the ${}^1S_0$ neutron-neutron scattering length, a_{nn}. This reaction produces three detectable particles in a final state, and the interaction of the photon with two emerging neutrons is so weak that the final state interaction (FSI) is absolutely dominated by the neutron-neutron (nn) scattering. As early as in 1951 Watson and Stuart [13] showed with quite simple dynamics that the corresponding photon spectrum very strongly depends on the properties of the nn interaction. Since then many theoretical efforts [14–21] combined with more and more precise measurements [22–32] have contributed decisively to our present day knowledge about a_{nn}. Detailed information about this rich field can be found in the review by Šlaus, Akaishi, and Tanaka [33] and in the more recent review by Gårdestig [34], where also complementary efforts [35,36] to determine a_{nn} from the ${}^2\mathrm{H}(n, np)n$ reaction were reported.

In order to extract a_{nn} from the $\pi^- + {}^2\mathrm{H} \to \gamma + n + n$ process, various theoretical frameworks were employed. The approach formulated and applied by Gibbs, Gibson, and Stephenson [16,17,37] used a nonrelativistic one-body transition operator containing relativistic corrections and a nn scattering wave function generated from the Reid soft-core potential [38]. The wave function was obtained in coordinate space, starting from the asymptotic region and then integrating towards smaller internucleon distances r. For $r \leqslant 1.4$ fm a fifth-degree polynomial with appropriate boundary conditions was used to represent the wave function. In order to minimize the error in the a_{nn} extraction, the calculations had to be restricted to small relative nn energies, that is, to the nn FSI peak region. While the first analysis of the experiment conducted at the Clinton P. Anderson Meson Physics Facility at Los Alamos (LAMPF) reported in Ref. [31] used theoretical cross sections derived with nonrelativistic phase space factors, the results published later in Ref. [32] were obtained with the corresponding relativistic formulas.

The second theoretical approach treated the nn rescatterings by means of Muskhelishvili-Omnès dispersion relations [39,40]. De Téramond and collaborators [18,19,41] considered various dynamical ingredients—like pion rescattering terms, off-shell effects and the impact of higher partial

 ©2018 American Physical Society

waves—and studied their importance for the extraction of a_{nn}. This theoretical framework was employed in the analysis of two experiments performed at SIN [27–30]. It is quite remarkable that the analyses of the SIN and LAMPF experiments led to equivalent results for a_{nn}, with very small theoretical errors of 0.3 fm in a_{nn}, even though they were based on different theories. Namely, the final result from the SIN experiment [30] was $a_{nn} = (-18.7 \pm 0.6)$ fm, representing a weighted mean of two data sets with systematic and theoretical errors added in quadrature. The corresponding result from the LAMPF experiment reported in Ref. [32] read $a_{nn} = [-18.63 \pm 0.27(\text{experiment}) \pm 0.30(\text{theory})]$ fm.

Further progress in the theoretical treatment of radiative pion capture reactions and the inverse process, pion photoproduction, was made in the framework of chiral effective field theory. In particular neutral pion photoproduction from a nucleon was studied by Bernard and collaborators [42] in the framework of heavy baryon chiral perturbation theory (HBCHPT). The same authors calculated also the one-loop corrections to the Kroll-Ruderman low-energy theorems for charged pion photoproduction at threshold in Ref. [43]. Within the same framework Fearing *et al.* [44] evaluated the transition amplitude for the photoproduction process away from threshold and obtained expressions for the s- and p-wave multipoles. They made connection with the radiative capture reaction at the cross section level via the detailed balance equation.

Several years later, Gårdestig and Phillips applied HBCHPT to the $\pi^- + {}^2\text{H} \to \gamma + n + n$ reaction [20,21,45] and for the first time used a consistent transition operator (with one- and two-body contributions) as well as the deuteron and nn scattering states. Namely, they worked in coordinate space and, starting from the asymptotic state, calculated the nn wave function solving the Schrödinger equation, which contained the lowest order chiral potential. For distances r smaller than a few fermis, a solution for the spherical well potential was chosen to account for the unknown short-distance physics. First calculations of Gårdestig and Phillips were carried out at next-to-next-to-leading order of chiral expansion and made it possible to extract a_{nn} with a precision at the 0.2 fm level.

Further investigations [21,45] at higher order of chiral expansion revealed important relations between the short-distance physics in a number of reactions on light nuclei, since the same axial isovector two-body contact term was found to contribute in the radiative pion capture on the deuteron, pion production in nucleon-nucleon (NN) scattering, triton β decay, proton-proton fusion, neutrino-deuteron scattering, muon capture on the deuteron, nucleon-deuteron scattering, and the $p + {}^3\text{He} \to {}^4\text{He} + e^+ + \nu_e$ (hep) process. The correlation found by Gårdestig and Phillips had direct impact on the accuracy with which a_{nn} was estimated, and allowed them to reduce the theoretical error to approximately 0.05 fm.

Investigation of the radiative (and nonradiative) negative pion capture in the three-nucleon (3N) bound states also started in the early 1950s. Even though this work prior to January 1976 is described in Ref. [2], we mention here a pioneering contribution by Messiah [46], who formulated a theoretical framework to deal with pion capture (not only radiative), discussed various dynamical aspects, and gave predictions for all the six reaction channels for the ^{3}He nucleus, which were, however, based on very crude approximations in the closure formulas.

Further theoretical efforts to describe radiative capture concentrated on the $\pi^- + {}^3\text{He} \to \gamma + {}^3\text{H}$ process. Some authors used very simple parametrizations of the ^{3}He and ^{3}H wave functions and the Kroll-Ruderman [47] form of the transition operator to calculate directly the pertinent nuclear matrix elements (see for example Ref. [48]). In other papers the so-called "elementary particle treatment of nuclei" was adopted [49–52]. Since the early measurements [53,54] yielded no absolute capture rates but rather relative probabilities of various processes, the theories tried to reproduce measured branching ratios. In particular the so-called Panofsky ratio—that is, the ratio of the probabilities of the charge exchange $\pi^- + {}^3\text{He} \to \pi^0 + {}^3\text{H}$ and radiative capture $\pi^- + {}^3\text{He} \to \gamma + {}^3\text{H}$ reactions—was studied in many papers, as exemplified by Refs. [55,56]. An important paper by Truöl *et al.* [57] not only brought new experimental data on the photon spectrum and several branching ratios but also corrections to the earlier theoretical predictions published in Refs. [48,52,58]. Using a formula from Ref. [59] and making a connection between the Gamow-Teller matrix element in triton β decay and the corresponding matrix elements in nonbreakup pion radiative capture on ^{3}He, the authors of Ref. [57] also provided a result for the $\pi^- + {}^3\text{He} \to \gamma + {}^3\text{H}$ capture rate.

The photon spectrum and the branching ratios from Ref. [57] were analyzed by Phillips and Roig [55]. Radiative breakup rates were calculated in the impulse approximation and FSI among the three nucleons was treated in the Amado model [60,61], by solving the Faddeev equations with a simple separable s-wave NN potential. The 3N bound states were not calculated consistently but had an analytical form, which allowed the authors to regulate strengths of the principal S-state, S'-state and D-state components. Despite these simplifications, Phillips and Roig could describe the shapes of the experimental photon spectrum and the branching ratios given in Ref. [57]. They also predicted the decisive role of FSI and the dominant contribution of the $\pi^- + {}^3\text{He} \to \gamma + n + d$ channel in the radiative breakup of ^{3}He.

In Ref. [62], the same authors made calculations for the $\pi^- + {}^3\text{H} \to \gamma + n + n + n$ capture reaction, later confronted with experimental results obtained by Bistirlich *et al.* [63] and (in an improved experiment) by Miller *et al.* [64]. This reaction allows one to study the 3N system in a pure total isospin $T = 3/2$ state and to search for resonant or even bound three-neutron states. None were found in the two above-mentioned LAMPF experiments and the smooth shape of the experimental photon spectrum was in satisfactory agreement with the theoretical predictions by Phillips and Roig. In particular FSI raised the theoretical spectrum obtained under a plane wave impulse approximation. Since later all pion beam facilities were shut down and the more recent theoretical work on radiative pion capture was focused on the single-nucleon and two-nucleon (2N) sector, no calculations for the 3N system with modern realistic nuclear forces have been performed.

Recently we have established a theoretical framework for the $A \leqslant 3$ muon capture reactions [65,66]. Important building blocks of this framework were cross-checked with the results

from Ref. [67], obtained using the hyperspherical harmonics formalism [68]. It has then become very natural to adapt our momentum space techniques for corresponding radiative capture reactions. Thus we provide, for the first time, predictions with consistent treatment of the initial and final nuclear states calculated from realistic 2N and 3N forces for the differential and total capture rates of the $\pi^- + {}^2\mathrm{H} \to \gamma + n + n$, $\pi^- + {}^3\mathrm{He} \to \gamma + {}^3\mathrm{H}$, $\pi^- + {}^3\mathrm{He} \to \gamma + n + d$, $\pi^- + {}^3\mathrm{He} \to \gamma + n + n + p$, and $\pi^- + {}^3\mathrm{H} \to \gamma + n + n + n$ reactions.

The paper is organized in the following way. In Sec. II we introduce the single-nucleon transition operator. In the following sections, we show selected results, concentrating on the photon spectra and total capture rates. In Sec. III, we start with the $\pi^- + {}^2\mathrm{H} \to \gamma + n + n$ reaction and demonstrate that our framework possesses the same sensitivity to a_{nn} as the older [30,32] and more recent, chiral calculations [20]. Our results concerning $\pi^- + {}^3\mathrm{He} \to \gamma + {}^3\mathrm{H}$ and breakup reactions with trinucleons are described in further sections, where we compare predictions obtained with different treatment of FSI. All our results for the total capture rates are shown together and compared to earlier theoretical predictions in Sec. VII. Finally, Sec. VIII contains our summary and outlook.

II. THE TRANSITION OPERATOR

The radiative capture process is treated in the same way as muon capture from the $1s$ atomic orbit. Namely, the initial state $\mid i\rangle$ comprises the K-shell pion wave function $\mid \psi\rangle$ and the initial nucleus state $\mid \Psi_i \mathbf{P}_i m_i\rangle$ with the three-momentum $\mathbf{P}_i$ and the spin projection m_i:

$$\mid i\rangle = \mid \psi\rangle \mid \Psi_i \mathbf{P}_i m_i\rangle. \tag{2.1}$$

In the final state $\mid f\rangle$ the photon occurs, described by the state $\mid \gamma \mathbf{p}_\gamma \boldsymbol{\epsilon}\rangle$ with the three-momentum $\mathbf{p}_\gamma$ and the polarization vector $\boldsymbol{\epsilon}$ perpendicular to $\mathbf{p}_\gamma$, accompanied by the final nuclear state $\mid \Psi_f \mathbf{P}_f m_f\rangle$ with the total three-momentum $\mathbf{P}_f$ and the set of spin projections m_f:

$$\mid f\rangle = \mid \gamma \mathbf{p}_\gamma \boldsymbol{\epsilon}\rangle \mid \Psi_f \mathbf{P}_f m_f\rangle. \tag{2.2}$$

We assume that the transition from the initial to final nuclear state is governed by the one-body operator. It is constructed by considering the $\pi^- + p \to \gamma + n$ process or its inverse, the negative pion photoproduction reaction: $\gamma + n \to \pi^- + p$. The most general Lorentz-invariant matrix elements for these reactions contains several terms [2]. In order to establish the connection between radiative pion capture and weak processes, such as muon capture, the hypothesis of partial conservation of axial-vector current (PCAC) is used. Additionally, since the pion is captured (or produced) essentially at rest, the soft-pion limit is calculated by setting $m_{\pi^-} \to 0$. In this limit only the so-called Kroll-Ruderman term j_{KR} [47] remains in the matrix element. Its simple nonrelativistic form is given in Ref. [2] as

$$j_{KR} = -ie\frac{g_A}{g_V}\frac{1}{f_\pi}\boldsymbol{\epsilon}\cdot\boldsymbol{\sigma}\tau_-, \tag{2.3}$$

where e, g_A, g_V, f_π, and $\boldsymbol{\sigma}$ are the elementary charge, axial-vector and vector coupling constants, the pion decay constant, and the nucleon spin operator, respectively. In the isospin formalism, also the isospin lowering operator, $\tau_- = (\tau_x - \mathrm{i}\tau_y)/2$, is introduced. In order to use numerical experience from our work on muon capture [65,66] we replace Eq. (2.3) by

$$j_{KR} = -i\frac{e}{f_\pi}\boldsymbol{\epsilon}\cdot\mathbf{j}_A, \tag{2.4}$$

where $\mathbf{j}_A$ is the single-nucleon axial current from Refs. [65,69]. This step is justified by the fact that for low momentum transfers the term $g_1^A\boldsymbol{\sigma}$ absolutely dominates momentum space matrix elements of $\mathbf{j}_A$, which contain additionally $(p/m)^2$ relativistic corrections and read

$$\begin{aligned}\langle \mathbf{p}' \mid \mathbf{j}_\mathrm{A}(1) \mid \mathbf{p}\rangle = \Bigg\{ & g_1^A\left(1 - \frac{(\mathbf{p}+\mathbf{p}')^2}{8M^2}\right)\boldsymbol{\sigma} + \frac{g_1^A}{4M^2}[(\mathbf{p}\cdot\boldsymbol{\sigma})\mathbf{p}' \\ & + (\mathbf{p}'\cdot\boldsymbol{\sigma})\mathbf{p} + i(\mathbf{p}\times\mathbf{p}')] \\ & + g_2^A(\mathbf{p}-\mathbf{p}')\frac{\boldsymbol{\sigma}\cdot(\mathbf{p}-\mathbf{p}')}{2M}\Bigg\}\tau_-,\end{aligned} \tag{2.5}$$

with $M \approx 939$ MeV being the nucleon mass. The detailed information about the nucleon form factors g_1^A and g_2^A is provided in Ref. [69].

In practice it is always possible to set $\hat{\mathbf{p}}_\gamma = -\hat{\mathbf{z}}$, which means that for a real photon only nuclear matrix elements of the transverse components of $\mathbf{j}_A$ (here represented in the spherical notation) need to be calculated:

$$N_{\pm 1} = \langle \Psi_f \mathbf{P}_f m_f \mid j_{A,\pm 1} \mid \Psi_i \mathbf{P}_i m_i\rangle. \tag{2.6}$$

The transversality condition implies also that the term in Eq. (2.5) proportional to g_2^A does not contribute.

The form of the transition operator employed in this article definitely leaves room for improvement. The assumptions leading to the Kroll-Ruderman result cannot be exactly fulfilled, not only because $m_{\pi^-} > 0$ but also due to the fact that protons in the nucleus are not at rest. That means that additional terms in the transition operator might play a role. Also the flaw caused by the inconsistency between the nuclear forces and the transition operator cannot be removed in the present framework. The current operator we employ constitutes, however, a good starting point for further investigations. A similar form of the current operator has been widely used in the literature; see for example [12].

Radiative pion capture by a single nucleon and the inverse, photoproduction process was studied in heavy baryon chiral perturbation theory in Refs. [42–44] and corrections to the Kroll-Ruderman low-energy theorem were calculated. One can also expect many-nucleon, most importantly 2N, contributions to the capture process. They were derived more recently by Gårdestig [20,21,45].

Our first predictions, however, are based on the single-nucleon transition operator and focus on other dynamical ingredients. Like for muon capture, we want to concentrate on FSI in the nuclear sector. To this end we calculate 2N and 3N scattering states using the AV18 NN potential [70] and the Urbana IX 3N force [71]. To the best of our knowledge, we provide, for the first time, consistent predictions for the total capture rates of the $\pi^- + {}^2\mathrm{H} \to \gamma + n + n$, $\pi^- + {}^3\mathrm{He} \to \gamma + {}^3\mathrm{H}$, $\pi^- + {}^3\mathrm{He} \to \gamma + n + d$, $\pi^- + {}^3\mathrm{He} \to \gamma + n +$

$n+p$, and $\pi^- + {}^3\mathrm{H} \to \gamma + n + n + n$ reactions, obtained with realistic 2N and 3N forces.

Many elements of our calculations for all the listed reactions are essentially the same as those performed for the corresponding muon capture reactions in Refs. [65,66]. In particular the formulas concerning kinematics can be directly used, if the muon mass is replaced by the negative pion mass. The radiative pion capture rates for the totally unpolarized reactions are also easily obtained from the corresponding expressions for the muon capture rates.

III. RESULTS FOR THE $\pi^- + {}^2\mathrm{H} \to \gamma + n + n$ REACTION

Our description of nuclear initial and final states is based on the nonrelativistic potentials and dynamical equations. It should then be used with the nonrelativistic kinematics. It is then mandatory to verify if the nonrelativistic approximations in the kinematics of the nuclear sector (the photon is of course treated relativistically) is justified. Clearly the pion is heavier than the muon, so pion absorption brings more energy to the nuclear system. Thus the comparisons of various results computed from the nonrelativistic and relativistic nuclear kinematics performed in Refs. [65,66] for muon capture had to be repeated with a new mass of the absorbed particle.

Starting from the energy and momentum conservation, we obtain first the maximal relativistic and nonrelativistic photon energies:

$$\left(E_\gamma^{\max,nn}\right)^{\mathrm{rel}} = \frac{1}{2}\left(-\frac{4{M_n}^2}{M_d+M_\pi} + M_d + M_\pi\right) \tag{3.1}$$

and

$$\left(E_\gamma^{\max,nn}\right)^{\mathrm{nrl}} = 2\sqrt{M_d M_n + M_\pi M_n - {M_n}^2} - 2M_n. \tag{3.2}$$

Assuming $M_p = 938.272$ MeV, $M_n = 939.565$ MeV, $M_\pi = 139.570$ MeV, and $M_d = M_p + M_n - 2.225$ MeV, we obtain $(E_\gamma^{\max,nn})^{\mathrm{rel}} = 131.459$ MeV and $(E_\gamma^{\max,nn})^{\mathrm{nrl}} = 131.454$ MeV, respectively, with a difference which is clearly negligible.

In Fig. 1, we demonstrate additionally that the kinematically allowed regions in the plane defined by the photon energy (E_γ) and the neutron kinetic energy (E_n) calculated relativistically and nonrelativistically essentially overlap, which means that the nonrelativistic kinematics can be safely used.

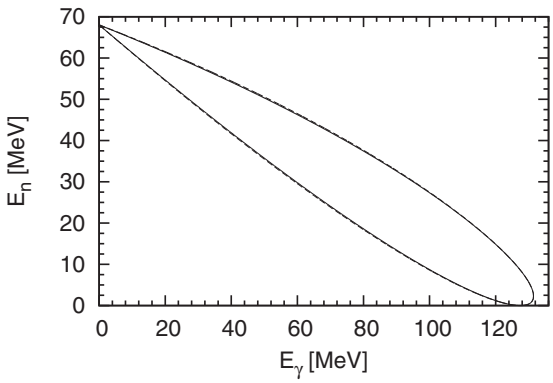

FIG. 1. The kinematically allowed region in the $E_\gamma - E_n$ plane calculated relativistically (solid curve) and nonrelativistically (dashed curve) for the $\pi^- + {}^2\mathrm{H} \to \gamma + n + n$ capture process. The lines practically overlap.

Taking the form of the transition matrix element into account, introducing the bosonic factors from the pion and photon fields, and evaluating the phase space factor in terms of the relative nn momentum, $\mathbf{p} = \frac{1}{2}(\mathbf{p}_1 - \mathbf{p}_2)$ ($\mathbf{p}_1$ and $\mathbf{p}_2$ are the two individual neutron momenta), we arrive at the following expression for the total unpolarized capture rate:

$$\begin{aligned}\Gamma_{nn} = {} & \frac{1}{2}\frac{1}{(2\pi)^2}\frac{2\pi\alpha}{f_\pi^2 M_\pi}\frac{\left(M_d'\alpha\right)^3}{\pi}\int_0^\pi d\theta_{p_\gamma}\sin\theta_{p_\gamma}\int_0^{2\pi} d\phi_{p_\gamma} \\ & \times \int_0^{E_\gamma^{\max,nn}} dE_\gamma E_\gamma \frac{1}{2} M_n p \int_0^\pi d\theta_p \sin\theta_p \int_0^{2\pi} d\phi_p \\ & \times \frac{1}{3}\sum_{m_d}\sum_{m_1,m_2}\left(|N_{nn,+1}(m_1,m_2,m_d)|^2\right. \\ & \left. + |N_{nn,-1}(m_1,m_2,m_d)|^2\right),\end{aligned} \tag{3.3}$$

where the factor $\frac{(M_d'\alpha)^3}{\pi}$ stems from the K-shell atomic wave function, $M_d' = \frac{M_d M_\pi}{M_d + M_\pi}$, $\alpha \approx \frac{1}{137}$ is the fine structure constant, and $p \equiv |\mathbf{p}| = p(E_\gamma)$. We use in our calculations $f_\pi \equiv \sqrt{2}F_\pi = 0.932 M_\pi$ [2].

We can further simplify Eq. (3.3), since for the unpolarized case only the relative angle between $\mathbf{p}$ and $\mathbf{p}_\gamma$ matters. Therefore we set $\hat{\mathbf{p}}_\gamma = -\hat{\mathbf{z}}$ and choose the azimuthal angle of the relative momentum $\phi_p = 0$, which leads to

$$\begin{aligned}\Gamma_{nn} = {} & \frac{1}{2}\frac{1}{(2\pi)^2}\frac{2\pi\alpha}{f_\pi^2 M_\pi}\frac{(M_d'\alpha)^3}{\pi} 4\pi \int_0^{E_\gamma^{\max,nn}} dE_\gamma E_\gamma \frac{1}{2} M_n p 2\pi \\ & \times \int_0^\pi d\theta_p \sin\theta_p \frac{1}{3}\sum_{m_d}\sum_{m_1,m_2}\left(|N_{nn,+1}(m_1,m_2,m_d)|^2\right. \\ & \left. + |N_{nn,-1}(m_1,m_2,m_d)|^2\right).\end{aligned} \tag{3.4}$$

For this direction of the three-momentum transferred to the nuclear system $\mathbf{Q} = -\mathbf{p}_\gamma$ and the process considered here with the real photon, we need only two spherical components of the current operator:

$$\begin{aligned} j_{+1} &\equiv -\frac{1}{\sqrt{2}}\left(j_{2N}^1 + i j_{2N}^2\right) \equiv -\frac{1}{\sqrt{2}}\left(j_{x2N} + i j_{y2N}\right), \\ j_{-1} &\equiv \frac{1}{\sqrt{2}}\left(j_{2N}^1 - i j_{2N}^2\right) \equiv \frac{1}{\sqrt{2}}\left(j_{x2N} - i j_{y2N}\right). \end{aligned} \tag{3.5}$$

Note that the same choice is also made for radiative pion capture in ^{3}He and ^{3}H. It provides the simplest relations between the total angular momentum projections of the initial and final nuclear systems. We generate the nuclear matrix elements $N_{nn,\pm1}(m_1,m_2,m_d)$ in momentum space [65], as summarized briefly in Appendix A. Although the three-dimensional formalism of Ref. [72] could be applied also to radiative pion capture in ^{2}H, in this article we discuss results obtained solely with a standard partial wave decomposition (PWD). In the calculations, we exclusively used the AV18 NN potential [70]. However, based on our experience from the muon capture process [65], we expect that predictions calculated with other realistic NN potentials would not differ significantly. The

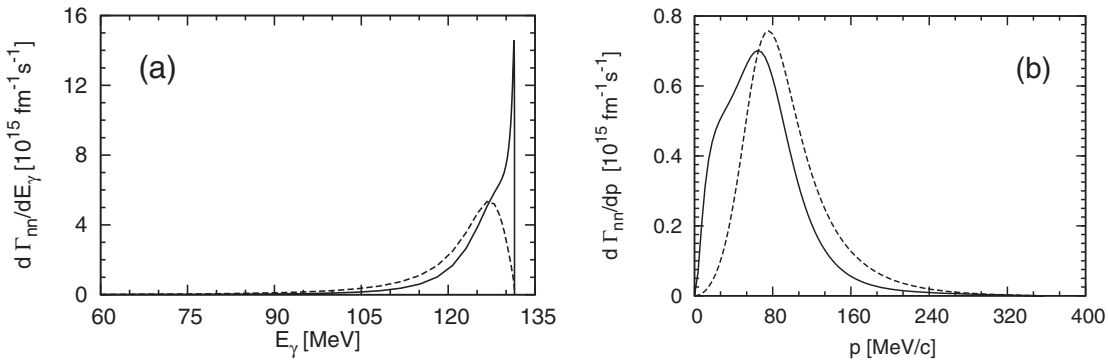

FIG. 2. The differential capture rate $d\Gamma_{nn}/dE_\gamma$ as a function of the photon energy E_γ (a) and the differential capture rate $d\Gamma_{nn}/dp$ as a function of the magnitude of the relative nn momentum p (b) for the $\pi^- + {}^2\mathrm{H} \to \gamma + n + n$ process, calculated with the AV18 potential [70] and using the transition operator from Eq. (2.4). The dashed curves show the plane wave results and the solid curves are used for the full results.

calculations have been performed including all partial wave states with the total angular momentum $j \leqslant 4$. In order to achieve fully converged results, 60 E_γ points and 50 θ_p points are used.

From Eq. (3.4), one can easily extract the differential capture rate $d\Gamma_{nn}/dE_\gamma$. This quantity is shown in the left panel of Fig. 2 for the plane wave part of $N_{nn,\pm1}(m_1, m_2, m_d)$ (PW, dashed line) and for the full $N_{nn,\pm1}(m_1, m_2, m_d)$ ("Full," solid line). When the full result for $N_{nn,\pm1}(m_1, m_2, m_d)$ is taken, a very narrow peak in the vicinity of $E_\gamma^{\max,nn}$ emerges. Here, the relative energy of the two-neutron system is very small, which explains strong rescattering effects in $d\Gamma_{nn}/dE_\gamma$. Another form of the differential capture rate, $d\Gamma_{nn}/dp$, is displayed in the right panel of Fig. 2, now as a function of the magnitude of the relative nn momentum. The transition between $d\Gamma_{nn}/dE_\gamma$ and $d\Gamma_{nn}/dp$ reads

$$\frac{d\Gamma_{nn}}{dp} = \frac{4p}{E_\gamma + 2M_n}\frac{d\Gamma_{nn}}{dE_\gamma}. \tag{3.6}$$

Despite the fact that the shapes of the differential rates shown in Fig. 2 for the plane wave and full dynamics are quite different, the corresponding integrated results for the total capture rate are rather similar. We obtain $\Gamma_{nn} = 0.318 \times 10^{15}\,\mathrm{s}^{-1}$ (PW) and $\Gamma_{nn} = 0.328 \times 10^{15}\,\mathrm{s}^{-1}$ (Full). Results of earlier calculations are displayed in Table I and discussed in Sec. VII.

The total capture rate Γ_{nn} can be also evaluated using other variables:

$$\begin{aligned}\Gamma_{nn} = {} & \frac{1}{2}\frac{1}{(2\pi)^2}\frac{2\pi\alpha}{f_\pi^2 M_\pi}\frac{(M_d'\alpha)^3}{\pi}\int_0^\pi d\theta_{p_\gamma}\sin\theta_{p_\gamma}\int_0^{2\pi} d\phi_{p_\gamma} \\ & \times \int_0^\pi d\theta_{p_1}\sin\theta_{p_1}\int_0^{2\pi} d\phi_{p_1} \\ & \times \int_0^{E_1^{\max}} dE_1 \frac{M_n^2 p_1 E_\gamma}{E_\gamma + M_n + p_1\cos\theta_{\gamma 1}} \\ & \times \frac{1}{3}\sum_{m_d}\sum_{m_1,m_2}(|N_{nn,+1}(m_1, m_2, m_d)|^2 \\ & + |N_{nn,-1}(m_1, m_2, m_d)|^2),\end{aligned} \tag{3.7}$$

where E_γ is the only physical solution of the nonrelativistic equation

$$\begin{aligned}& E_\gamma^2 + 2(M_n + p_1\cos\theta_{\gamma 1})E_\gamma \\ & + 2\left[p_1^2 - M_n(M_d + M_\pi - 2M_n)\right] = 0,\end{aligned} \tag{3.8}$$

and it depends on the magnitude of the detected neutron momentum, p_1, as well as on the angle between the detected neutron and photon momentum, $\theta_{\gamma 1}$. Note that the maximal neutron energy $E_1^{\max}$, which equals $\frac{1}{2}(M_d + M_\pi - 2M_n)$, does not depend on $\theta_{\gamma 1}$. Like Eq. (3.3), also Eq. (3.7) can be simplified, choosing $\hat{\mathbf{p}}_\gamma = -\hat{\mathbf{z}}$ and the azimuthal angle of the neutron momentum $\phi_1 = 0$.

The building block of Eq. (3.7) is the differential capture rate

$$\begin{aligned}& d^5\Gamma_{nn}/(d\hat{\mathbf{p}}_\gamma d\hat{\mathbf{p}}_1 dE_1) \\ & = \frac{1}{2}\frac{1}{(2\pi)^2}\frac{2\pi\alpha}{f_\pi^2 M_\pi}\frac{(M_d'\alpha)^3}{\pi}\frac{M_n^2 p_1 E_\gamma}{E_\gamma + M_n + p_1\cos\theta_{\gamma 1}} \\ & \times \frac{1}{3}\sum_{m_d}\sum_{m_1,m_2}(|N_{nn,+1}(m_1, m_2, m_d)|^2 \\ & + |N_{nn,-1}(m_1, m_2, m_d)|^2).\end{aligned} \tag{3.9}$$

TABLE I. The total radiative capture rate Γ_{nn} in $10^{15}\,\mathrm{s}^{-1}$ for the $\pi^- + {}^2\mathrm{H} \to \gamma + n + n$ reaction calculated with the AV18 [70] NN potential and the nonrelativistic single-nucleon transition operator (2.5). Plane wave impulse approximation based results (PW) and the predictions including nn FSI (Full) are displayed together with earlier theoretical predictions.

PW	0.318	
Full	0.328	
Earlier theoretical predictions:		
Ref. [76] (1966)	0.332	0.4 (corrected in Ref. [77])
Ref. [77] (1976)	0.375	(based on pion photoproduction data)
Ref. [77] (1976)	0.383	(based on soft-pion limit)
Ref. [17] (1977)	0.420 ± 0.05	

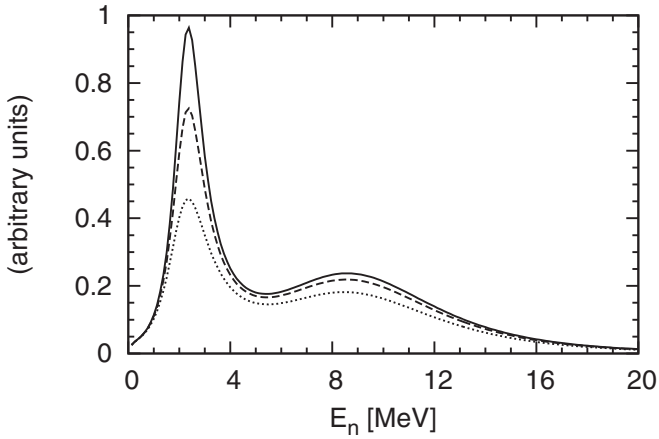

FIG. 3. The differential capture rate $d^5\Gamma_{nn}/(d\hat{\mathbf{p}}_\gamma d\hat{\mathbf{p}}_1 dE_1)$ calculated with the AV18 potential [70] and using the transition operator from Eq. (2.4) as a function of the neutron energy $E_n \equiv E_1$ for three different angles between the emitted photon and neutron momentum $\theta_{\gamma 1}$: 179° (solid line), 175° (dashed line), and 171° (dotted line). All the results correspond to $a_{nn} = -18.8$ fm.

As early as in 1951 Watson and Stuart [13] showed with quite simple dynamics that the corresponding photon spectrum is very sensitive to the properties of the low-energy *nn* interaction. Since then many calculations [14–21,32,41], summarized in Ref. [34], have also demonstrated that this capture process can be used to study the properties of low-energy *nn* scattering.

Also results of our calculations (see Figs. 3 and 4) show that the photon spectrum has two salient peaks: the *nn* FSI peak around $E_n \equiv E_1 = 2$ MeV and the so-called QFS peak arising from the quasifree $\pi^- p$ process around $E_n = 9$ MeV. From Fig. 3, it is clear that heights of the peaks increase with

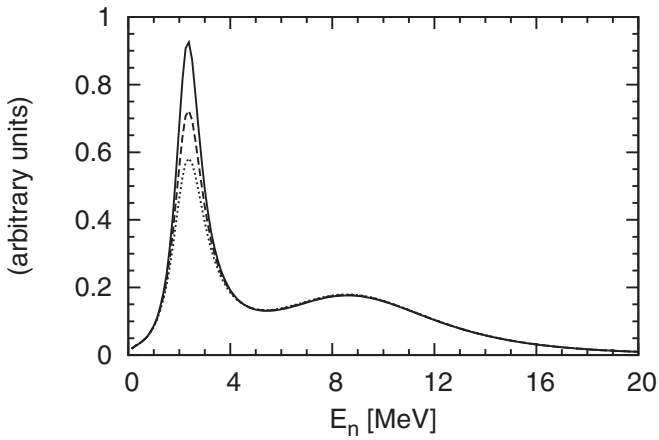

FIG. 4. The differential capture rate $d^5\Gamma_{nn}/(d\hat{\mathbf{p}}_\gamma d\hat{\mathbf{p}}_1 dE_1)$ as a function of the neutron energy $E_n \equiv E_1$ calculated with the transition operator from Eq. (2.4) and with three versions of the AV18 potential [70] yielding different a_{nn} values: -21.8 fm (solid line), -18.8 fm (dashed line) and -16.5 fm (dotted line). All the results correspond to $\theta_{\gamma 1} = 179°$.

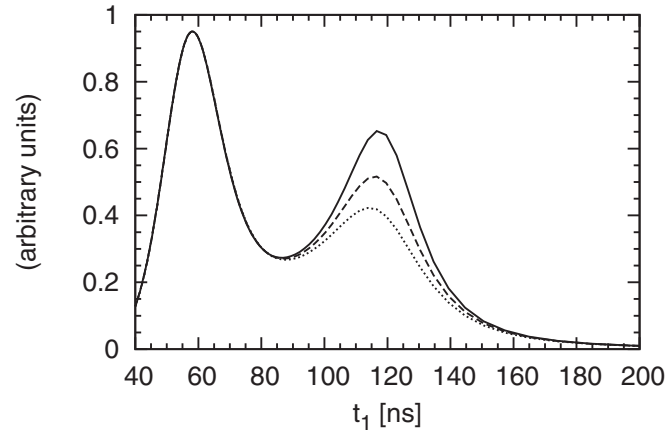

FIG. 5. The differential capture rate $d^5\Gamma_{nn}/(d\hat{\mathbf{p}}_\gamma d\hat{\mathbf{p}}_1 dt_1)$ (neutron time-of-flight spectrum for a flight path of 2.55 m) obtained from the results shown in Fig. 4. The results corresponding to different a_{nn} values, represented by the same lines as in Fig. 4, are normalized at the (left) QFS peak.

increasing $\theta_{\gamma 1}$. More importantly, for fixed $\theta_{\gamma 1}$ small variations of the ${}^1S_0$ *nn* interaction lead to quite visible changes in the FSI peak. We study this effect, performing additional calculations with the altered nn AV18 potential whose ${}^1S_0$ matrix elements are multiplied by the factors 1.01 and 0.99. This leads to the following changes of the a_{nn} values: for the stronger version of the potential we get $a_{nn} = -21.8$ fm, while for the weakened force $a_{nn} = -16.5$ fm. (The original value is $a_{nn} = -18.8$ fm.) The primary and modified neutron spectra are displayed in Fig. 4 and we see that the FSI peak becomes higher if the absolute value of a_{nn} grows. Note that in all these calculations the nn AV18 potential was used without electromagnetic contributions.

Actually, in order to minimize systematic uncertainties in the a_{nn} extraction, the very shape of the neutron time-of-flight spectrum in the area corresponding to the FSI peak is considered [30,32]. The nonrelativistic relation between the time-of-flight variable t_1 and the kinetic energy of the neutron E_n reads

$$E_n = \frac{1}{2} M_n s^2 \frac{1}{t_1^2}, \tag{3.10}$$

where s is the flight path to the neutron detector. A simple step then leads to the neutron time-of-flight spectrum demonstrated in Fig. 5 (for $s = 2.55$ m) for the same three values of a_{nn}:

$$\begin{aligned} &d^5\Gamma_{nn}/(d\hat{\mathbf{p}}_\gamma d\hat{\mathbf{p}}_1 dt_1) \\ &= \frac{1}{2}\frac{1}{(2\pi)^2}\frac{2\pi\alpha}{f_\pi^2 M_\pi}\frac{(M_d'\alpha)^3}{\pi}\frac{M_n p_1^3 E_\gamma}{t_1(E_\gamma + M_n + p_1\cos\theta_{\gamma 1})} \\ &\quad\times\frac{1}{3}\sum_{m_d}\sum_{m_1,m_2}(|N_{nn,+1}(m_1,m_2,m_d)|^2 \\ &\quad + |N_{nn,-1}(m_1,m_2,m_d)|^2). \end{aligned} \tag{3.11}$$

Equation (3.11) can be compared with the relativistic formula from Eq. (3) in Ref. [20].

We do not intend here to work on the extraction of a_{nn} with our present theory. Before moving to calculations with 3N systems we wanted to make sure that our framework possesses the same important features as the calculations used in the old and more recent analyses of the $\pi^- + {}^2\mathrm{H} \to \gamma + n + n$ process [14–20,32].

IV. RESULTS FOR THE $\pi^- + {}^3\mathrm{He} \to \gamma + {}^3\mathrm{H}$ REACTION

In this case, we deal with two-body kinematics and we can compare the photon energy calculated nonrelativistically and using relativistic equations. The relativistic result, based on

$$M_\pi + M_{^3\mathrm{He}} = E_\gamma + \sqrt{E_\gamma^2 + M_{^3\mathrm{H}}^2}, \tag{4.1}$$

reads

$$(E_\gamma)^{\mathrm{rel}} = \frac{(M_{^3\mathrm{He}} + M_\pi)^2 - M_{^3\mathrm{H}}^2}{2(M_{^3\mathrm{He}} + M_\pi)}. \tag{4.2}$$

In the nonrelativistic case, we start with

$$M_\pi + M_{^3\mathrm{He}} = E_\gamma + M_{^3\mathrm{H}} + \frac{E_\gamma^2}{2M_{^3\mathrm{H}}} \tag{4.3}$$

and arrive at

$$(E_\gamma)^{\mathrm{nrl}} = -M_{^3\mathrm{H}} + \sqrt{M_{^3\mathrm{H}}[-M_{^3\mathrm{H}} + 2(M_{^3\mathrm{He}} + M_\pi)]}. \tag{4.4}$$

Again the obtained numerical values, $(E_\gamma)^{\mathrm{rel}} = 135.760$ MeV and $(E_\gamma)^{\mathrm{nrl}} = 135.743$ MeV, are very close to each other.

For this reaction we calculate only the total capture rate

$$\begin{aligned}\Gamma_{^3\mathrm{H}} = {} & \frac{1}{2}\frac{1}{(2\pi)^2}\mathcal{R}\frac{2\pi\alpha}{f_\pi^2 M_\pi E_\gamma}\frac{\left(2M'_{^3\mathrm{He}}\alpha\right)^3}{\pi}\rho \\ & \times 4\pi\frac{1}{2}\sum_{m_{^3\mathrm{He}}}\sum_{m_{^3\mathrm{H}}}(|N_{+1}(m_{^3\mathrm{H}}, m_{^3\mathrm{He}})|^2 \\ & + |N_{-1}(m_{^3\mathrm{H}}, m_{^3\mathrm{He}})|^2),\end{aligned} \tag{4.5}$$

where the factor $\frac{(2M'_{^3\mathrm{He}}\alpha)^3}{\pi}$, as in the deuteron case, comes from the K-shell atomic wave function and $M'_{^3\mathrm{He}} = \frac{M_{^3\mathrm{He}}M_\pi}{M_{^3\mathrm{He}}+M_\pi}$. For the unpolarized reaction the angular integration over the photon momenta leads to the 4π factor, and in all the considered cases we set $\hat{\mathbf{p}}_\gamma = -\hat{\mathbf{z}}$. The phase space factor ρ is

$$\rho = \frac{E_\gamma^2}{1 + \frac{E_\gamma}{\sqrt{E_\gamma^2 + M_{^3\mathrm{H}}^2}}} \approx E_\gamma^2\left(1 - \frac{E_\gamma}{M_{^3\mathrm{H}}}\right). \tag{4.6}$$

As in muon capture, the additional factor $\mathcal{R}$ stems from the overlap of the $1s$ solution of the Schrödinger equation and the ^{3}He charge distribution [73]. For the Hamiltonian used in the present paper it has been calculated explicitly in Ref. [67] with the result $\mathcal{R} = 0.98$, very close to the value calculated from the experimental ^{3}He charge density and commonly used in the literature [67,73]. The corresponding correction in the deuteron case is much smaller and therefore has been neglected.

The nuclear matrix elements involve the initial ^{3}He and final ^{3}H states,

$$\begin{aligned}& N_{\pm1}(m_{^3\mathrm{H}}, m_{^3\mathrm{He}}) \\ & \equiv \langle \Psi_{^3\mathrm{H}}\mathbf{P}_f = -\mathbf{p}_\gamma\ m_{^3\mathrm{H}} \mid j_{A,\pm1} \mid \Psi_{^3\mathrm{He}}\mathbf{P}_i = 0\ m_{^3\mathrm{He}}\rangle,\end{aligned} \tag{4.7}$$

and are obtained employing our standard PWD techniques [65,74]. Basic information about the way we calculate the 3N bound states is deferred to Appendix B.

Our results for this process are obtained for two cases. When we generate the ^{3}He and ^{3}H wave functions using the AV18 NN potential only, we get $\Gamma_{^3\mathrm{H}} = 2.059 \times 10^{15}\ \mathrm{s}^{-1}$. For the wave functions calculated with the AV18 NN potential augmented by the Urbana IX 3N force, the rate is slightly reduced to $\Gamma_{^3\mathrm{H}} = 2.013 \times 10^{15}\ \mathrm{s}^{-1}$. These predictions are compared with the results of earlier calculations in Table II and discussed in Sec. VII.

TABLE II. Rates Γ in $10^{15}\ \mathrm{s}^{-1}$ for radiative pion capture in ^{3}He and ^{3}H calculated with the AV18 [70] NN potential and the nonrelativistic single-nucleon transition operator (2.5). Results obtained using the plane wave impulse approximation (PW 2NF), with consistent treatment of the initial and final nuclear states based on 2N forces only (Full 2NF), and, additionally, employing the Urbana IX [71] 3N force (Full 2NF+3NF) are presented. Earlier theoretical predictions are also displayed.

$\pi^- + {}^3\mathrm{He} \to \gamma + {}^3\mathrm{H}$	$\Gamma_{^3\mathrm{H}}$	
Full 2NF	2.059	
Full 2NF+3NF	2.132	
Earlier theoretical predictions:		
Ref. [58] (1962)	8.32	4.28 (corrected in Ref. [57])
Ref. [48] (1965)	0.97	3.88 (corrected in Ref. [57])
Ref. [51] (1968)	2.32	
Ref. [52] (1970)	3.37	2.25 (corrected in Ref. [57])
Ref. [57] (1974)	3.60	
Ref. [55] (1974)	3.1–3.7	
Ref. [56] (1978)	3.30	
$\pi^- + {}^3\mathrm{He} \to \gamma + n + d$	Γ_{nd}	
PW 2NF	5.201	
Full 2NF	2.013	
Full 2NF+3NF	1.840	
$\pi^- + {}^3\mathrm{He} \to \gamma + n + n + p$	Γ_{nnp}	
PW 2NF	3.816	
Full 2NF	0.659	
Full 2NF+3NF	0.615	
$(\Gamma_{nd} + \Gamma_{nnp})/\Gamma_{^3\mathrm{H}}$		
Full 2NF	1.30	
Full 2NF+3NF	1.15	
Earlier theoretical predictions:		
Ref. [55] (1974)	0.84–1.27	
Experimental data:		
Ref. [57] (1974)	1.12 ± 0.05	
$\pi^- + {}^3\mathrm{H} \to \gamma + n + n + n$	Γ_{nnn}	
PW 2NF	0.117	
Full 2NF	0.141	
Full 2NF+3NF	0.128	
Earlier theoretical predictions:		
Ref. [62] (1975)	0.07	

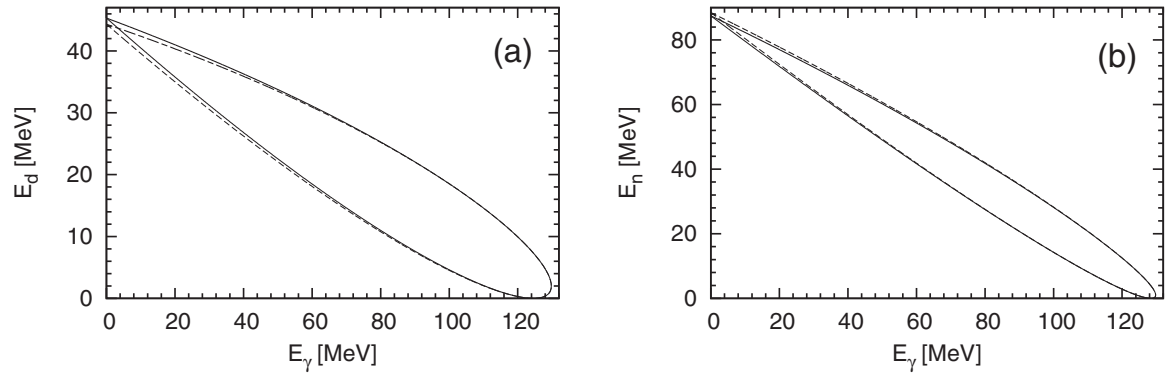

FIG. 6. The kinematically allowed region in the $E_\gamma - E_d$ (a) and $E_\gamma - E_n$ (b) plane calculated relativistically (solid curve) and nonrelativistically (dashed curve) for the $\pi^- + {}^3\mathrm{He} \to \gamma + n + d$ process. The lines overlap except for small photon energies.

V. RESULTS FOR THE $\pi^- + {}^3\mathrm{He} \to \gamma + n + d$ AND $\pi^- + {}^3\mathrm{He} \to \gamma + n + n + p$ REACTIONS

The kinematics of the $\pi^- + {}^3\mathrm{He} \to \gamma + n + d$ and $\pi^- + {}^3\mathrm{He} \to \gamma + n + n + p$ reactions is treated exactly in the same way as in muon capture on ^{3}He [65], so we can immediately evaluate the maximal photon energies for the two breakup channels as

$$\left(E_\gamma^{\max,nd}\right)^{\mathrm{rel}} = \frac{(M_{^3\mathrm{He}} - M_d + M_\pi - M_n)(M_{^3\mathrm{He}} + M_d + M_\pi + M_n)}{2(M_{^3\mathrm{He}} + M_\pi)}, \tag{5.1}$$

$$\left(E_\gamma^{\max,nnp}\right)^{\mathrm{rel}} = \frac{M_{^3\mathrm{He}}{}^2 + 2M_{^3\mathrm{He}}M_\pi + M_\pi{}^2 - (2M_n + M_p)^2}{2(M_{^3\mathrm{He}} + M_\pi)}, \tag{5.2}$$

$$\left(E_\gamma^{\max,nd}\right)^{\mathrm{nrl}} = \sqrt{(M_d + M_n)(2M_{^3\mathrm{He}} + 2M_\pi - M_d - M_n)} - M_d - M_n, \tag{5.3}$$

$$\left(E_\gamma^{\max,nnp}\right)^{\mathrm{nrl}} = \sqrt{(M_p + 2M_n)(2M_{^3\mathrm{He}} + 2M_\pi - 2M_n - M_p)} - 2M_n - M_p. \tag{5.4}$$

The numerical values are the following: $(E_\gamma^{\max,nd})^{\mathrm{rel}} = 129.794$ MeV, $(E_\gamma^{\max,nd})^{\mathrm{nrl}} = 129.792$ MeV, $(E_\gamma^{\max,nnp})^{\mathrm{rel}} = 127.668$ MeV, and $(E_\gamma^{\max,nnp})^{\mathrm{nrl}} = 127.667$ MeV. The kinematically allowed regions in the planes spanned by the photon energy (E_γ) and the deuteron kinetic energy (E_d) or the neutron kinetic energy (E_n) for the two-body breakup of ^{3}He are shown in Fig. 6. For both cases, lines obtained with the relativistic and nonrelativistic kinematics fully overlap except for very small photon energies. The same is also true for the three-body breakup, as demonstrated in Fig. 7 for the allowed region in the plane given by the photon energy and the proton kinetic energy (E_p). In this case the minimal proton kinetic energy is greater than zero for $E_\gamma > E_\gamma^{\mathrm{2sol}}$ (see the inset in Fig. 7), which means that $0 < E_p^{\mathrm{low}} < E_p < E_p^{\mathrm{high}}$ for $E_\gamma^{\mathrm{2sol}} < E_\gamma < E_\gamma^{\max,nnp}$, with boundary values E_p^{low} and E_p^{high}. The values of E_γ^{2sol} based on the relativistic kinematics,

$$\left(E_\gamma^{\mathrm{2sol}}\right)^{\mathrm{rel}} = \frac{(M_{^3\mathrm{He}}+M_\pi)(M_{^3\mathrm{He}} + M_\pi - 2M_p) - 4M_n{}^2 + M_p{}^2}{2(M_{^3\mathrm{He}}+M_\pi - M_p)} \tag{5.5}$$

and nonrelativistic one,

$$\left(E_\gamma^{\mathrm{2sol}}\right)^{\mathrm{nrl}} = 2\left(\sqrt{M_{^3\mathrm{He}}M_n + M_\pi M_n - M_n{}^2 - M_n M_p} - M_n\right), \tag{5.6}$$

yield very similar numerical values: 126.318 and 126.314 MeV, respectively. All these results clearly show that the

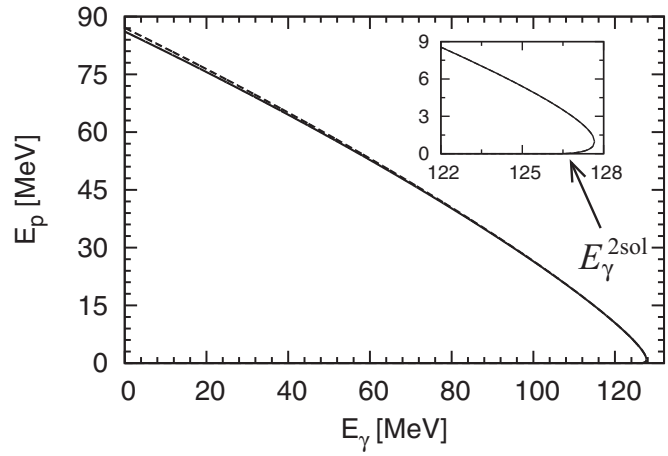

FIG. 7. The kinematically allowed region in the $E_\gamma - E_p$ plane calculated relativistically (solid curve) and nonrelativistically (dashed curve) for the $\pi^- + {}^3\mathrm{He} \to \gamma + n + n + p$ process. The inset focuses on the highest photon energy region. Note that the minimal proton kinetic energy is zero for $E_\gamma \leqslant E_\gamma^{\mathrm{2sol}}$. The lines practically overlap except for very small photon energies.

nonrelativistic kinematics can be safely used also for the breakup channels.

Using standard steps we obtain the formulas for the total capture rates. In the case of the two-body breakup it reads

$$\Gamma_{nd} = \frac{1}{2}\frac{1}{(2\pi)^2}\frac{2\pi\alpha}{f_\pi^2 M_\pi}\mathcal{R}\frac{\left(2M'_{^3\mathrm{He}}\alpha\right)^3}{\pi}4\pi \times \int_0^{E_\gamma^{\max,nd}} dE_\gamma E_\gamma \frac{2}{3}Mq_0\frac{1}{3}\int_0^\pi d\theta_{q_0}\sin\theta_{q_0}2\pi \times\frac{1}{2}\sum_{m_{^3\mathrm{He}}}\sum_{m_n,m_d}\left(|N_{nd,+1}(m_n,m_d,m_{^3\mathrm{He}})|^2 + |N_{nd,-1}(m_n,m_d,m_{^3\mathrm{He}})|^2\right), \tag{5.7}$$

where we used the relative neutron-deuteron momentum

$$\mathbf{q}_0 \equiv \frac{2}{3}\left(\mathbf{p}_n - \frac{1}{2}\mathbf{p}_d\right), \tag{5.8}$$

given in terms of the final neutron ($\mathbf{p}_n$) and deuteron ($\mathbf{p}_d$) momenta, to evaluate Γ_{nd}. For the $\pi^- + {}^3\mathrm{He} \to \gamma + n + n + p$ reaction we obtain in a similar way

$$\Gamma_{nnp} = \frac{1}{2}\frac{1}{(2\pi)^2}\frac{2\pi\alpha}{f_\pi^2 M_\pi}\mathcal{R}\frac{\left(2M'_{^3\mathrm{He}}\alpha\right)^3}{\pi}4\pi \int_0^{E_\gamma^{\max,nnp}} dE_\gamma E_\gamma \frac{1}{3}\int_0^\pi d\theta_q \sin\theta_q 2\pi \int_0^\pi d\theta_p \sin\theta_p \int_0^{2\pi} d\phi_p \int_0^{p^{\max}} dp p^2 \frac{2}{3}Mq \frac{1}{2}\sum_{m_{^3\mathrm{He}}}\sum_{m_1,m_2,m_p}\left(|N_{nnp,+1}(m_1,m_2,m_p,m_{^3\mathrm{He}})|^2 + |N_{nnp,-1}(m_1,m_2,m_p,m_{^3\mathrm{He}})|^2\right). \tag{5.9}$$

Here the integral is expressed in terms of the Jacobi relative momenta $\mathbf{p}$ and $\mathbf{q}$, that is,

$$\mathbf{p} \equiv \frac{1}{2}(\mathbf{p}_1 - \mathbf{p}_2),$$
$$\mathbf{q} \equiv \frac{2}{3}\left(\mathbf{p}_p - \frac{1}{2}(\mathbf{p}_1 + \mathbf{p}_2)\right), \tag{5.10}$$

obtained from the proton momentum ($\mathbf{p}_p$) and the momenta of the two neutrons ($\mathbf{p}_1$ and $\mathbf{p}_2$). In Eq. (5.9) $p^{\max}$ is a function of E_γ and $q \equiv |\mathbf{q}| = q(E_\gamma, p)$ [66]. Note that we used the same geometrical arguments as before to simplify the angular integrations in Eqs. (5.7) and (5.9).

The crucial matrix elements

$$N_{nd,\pm1}(m_n,m_d,m_{^3\mathrm{He}}) \equiv \langle \Psi_{nd}^{(-)}\mathbf{P}_f = -\mathbf{p}_\gamma\ m_n m_d \mid j_{A,\pm1} \mid \Psi_{^3\mathrm{He}}\mathbf{P}_i = 0\ m_{^3\mathrm{He}}\rangle \tag{5.11}$$

and

$$N_{nnp,\pm1}(m_1,m_2,m_p,m_{^3\mathrm{He}}) \equiv \langle \Psi_{nnp}^{(-)}\mathbf{P}_f = -\mathbf{p}_\gamma\ m_1 m_2 m_p \mid j_{A,\pm1} \mid \Psi_{^3\mathrm{He}}\mathbf{P}_i = 0\ m_{^3\mathrm{He}}\rangle \tag{5.12}$$

are calculated in momentum space, as explained concisely in Appendix B. We use the numerical framework developed in Refs. [74,75]. Also in Ref. [74] the detailed definitions of various 3N dynamics can be found.

Since the convergence of our PWD-based results with respect to the total subsystem angular momentum j and the total 3N angular momentum J was discussed in Ref. [65], we can start the discussion of our predictions with Fig. 8, where, for the $\pi^- + {}^3\mathrm{He} \to \gamma + n + d$ reaction, we compare in the left panel results of calculations employing various 3N dynamics: symmetrized plane wave approximation obtained with the AV18 NN potential, consistent calculations of the initial and final nuclear states with the AV18 interaction only, and calculations based on the Hamiltonian containing additionally the Urbana IX 3N force. The results are qualitatively quite similar to the ones obtained for muon capture. The three differential capture rates $d\Gamma_{nd}/dE_\gamma$ rise very slowly with the photon energy and form a single maximum close to the maximal photon energy. This maximum is higher and broader for the plane wave case. Effects introduced by FSI are very important and, in the maximum, reduce the full $d\Gamma_{nd}/dE_\gamma$ to about one-half of the plane wave prediction. The inclusion of the 3N force lowers the peak further by about 14%.

The FSI effects are even stronger for the $\pi^- + {}^3\mathrm{He} \to \gamma + n + n + p$ reaction, as displayed in the right panel of Fig. 8 for the differential rate $d\Gamma_{nnp}/dE_\gamma$. The reduction factor is already about 4.5 for the case without 3N force. The 3N force has roughly the same effect as in the two-body breakup case. In Ref. [65] we suggested that this might be a consequence of the overprediction of the $A = 3$ radii when 3N interaction is neglected.

Since the values of $d\Gamma_{nnp}/dE_\gamma$ are much smaller (by a factor of 5) than $d\Gamma_{nd}/dE_\gamma$, at least in the peak area, the picture shown in the left panel of Fig. 9 for the total breakup capture rate, $d\Gamma_{br}/dE_\gamma = d\Gamma_{nd}/dE_\gamma + d\Gamma_{nnp}/dE_\gamma$, is similar to the one for $d\Gamma_{nd}/dE_\gamma$. Finally, in the right panel of Fig. 9, we show the contributions from the two-body and three-body breakup channels calculated with our full dynamics, that

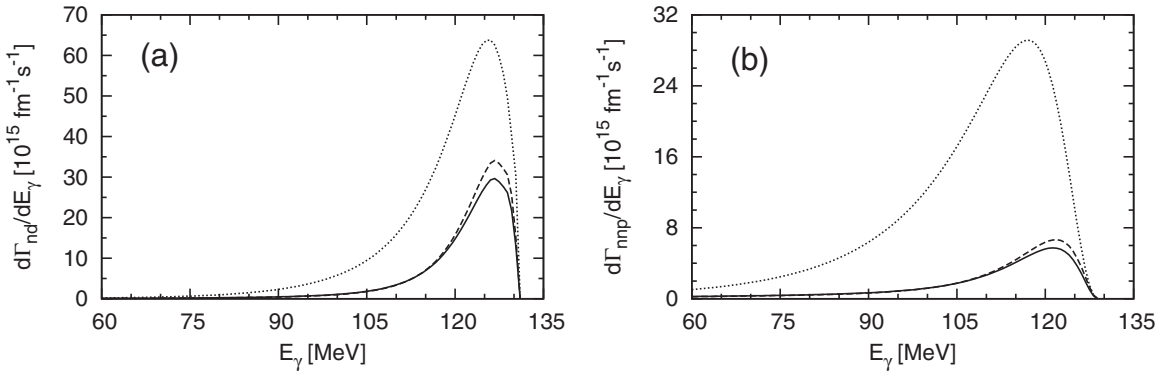

FIG. 8. The differential capture rate $d\Gamma_{nd}/dE_\gamma$ for the $\pi^- + {}^3\mathrm{He} \to \gamma + n + d$ process (a) and the differential capture rate $d\Gamma_{nnp}/dE_\gamma$ for the $\pi^- + {}^3\mathrm{He} \to \gamma + n + n + p$ reaction (b) as a function of the photon energy, calculated with the single-nucleon transition operator and with different treatment of 3N dynamics: taking the symmetrized plane wave (SPW) approximation (dotted line) and calculating the initial and final 3N states without (dashed curve) and with (solid line) 3N force. The calculations are based on the AV18 NN potential [70] and the Urbana IX 3N force [71].

is, including the 3N force. This figure clearly demonstrates that the breakup is dominated by the two-body channel. The corresponding predictions for the total Γ_{nd} and Γ_{nnp} capture rates are presented in Table II together with earlier theoretical predictions and experimental information about the relative probability of the breakup and nonbreakup radiative capture. These results will be discussed in Sec. VII.

VI. RESULTS FOR THE $\pi^- + {}^3\mathrm{H} \to \gamma + n + n + n$ REACTION

The kinematically allowed region in the E_γ-E_n plane for the three-body breakup of ^{3}H is shown in Fig. 10. As in the $\pi^- + {}^3\mathrm{He} \to \gamma + n + n + p$ capture process, we show the border lines based on the relativistic and nonrelativistic kinematics and evaluate correspondingly the maximal photon energy relativistically $(E_\gamma^{\max,nnn})^{\mathrm{rel}} = 126.940$ MeV and nonrelativistically $(E_\gamma^{\max,nnn})^{\mathrm{nrl}} = 126.939$ MeV. For completeness we give also values of $E_\gamma^{2\mathrm{sol}}$: $(E_\gamma^{2\mathrm{sol}})^{\mathrm{rel}} = 125.604$ MeV and $(E_\gamma^{2\mathrm{sol}})^{\mathrm{nrl}} = 125.600$ MeV. As expected, the kinematics of this reaction can be described using the nonrelativistic formulas in the nuclear sector, consistent with the nonrelativistic dynamics.

In the calculations of the three-neutron continuum only the *nn* version of the AV18 potential [70] appears. The nuclear Hamiltonian contains the same Urbana IX 3N force [71]. The formula for the total Γ_{nnn} capture rate,

$$\begin{aligned}\Gamma_{nnn} = {} & \frac{1}{2}\frac{1}{(2\pi)^2}\frac{2\pi\alpha}{f_\pi^2 M_\pi}\frac{\left(M'_{^3\mathrm{H}}\alpha\right)^3}{\pi} 4\pi \int_0^{E_\gamma^{\max,nnn}} dE_\gamma E_\gamma \frac{2}{3} Mq \frac{1}{9} \\ & \times \int_0^\pi d\theta_q \sin\theta_q 2\pi \int_0^\pi d\theta_p \sin\theta_p \int_0^{2\pi} d\phi_p \int_0^{p^{\max}} dp\, p^2 \\ & \times \frac{1}{2}\sum_{m_{^3\mathrm{H}}} \sum_{m_1,m_2,m_3} \left(|N_{nnn,+1}(m_1,m_2,m_3,m_{^3\mathrm{H}})|^2\right. \\ & \left. + |N_{nnn,-1}(m_1,m_2,m_3,m_{^3\mathrm{H}})|^2\right), \end{aligned} \tag{6.1}$$

is a modification of Eq. (5.9), taking into account that, as in the deuteron case, $Z = 1, \mathcal{R} = 1$, and that there are three identical particles in the final state.

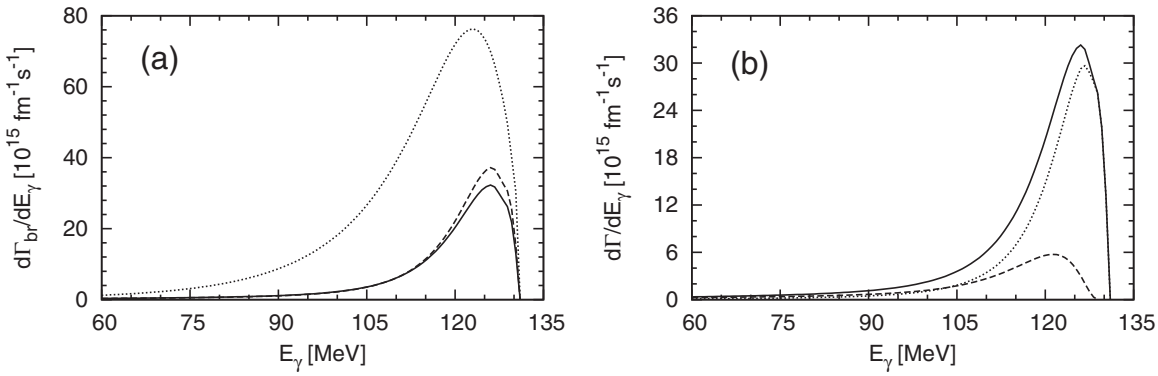

FIG. 9. As in Fig. 8 but for (a) the differential breakup capture rate $d\Gamma_{br}/dE_\gamma = d\Gamma_{nd}/dE_\gamma + d\Gamma_{nnp}/dE_\gamma$. In (b) the two-body $d\Gamma_{nd}/dE_\gamma$ (dotted curve) and three-body $d\Gamma_{nnp}/dE_\gamma$ (dashed curve) breakup contributions to the differential breakup radiative pion capture rate $d\Gamma_{br}/dE_\gamma$ (solid curve) are displayed as a function of the photon energy. They are obtained with the single-nucleon transition operator and with full 3N dynamics (including 3N force in the initial and final nuclear states). As before, the calculations are based on the AV18 NN potential [70] and the Urbana IX 3N force [71].

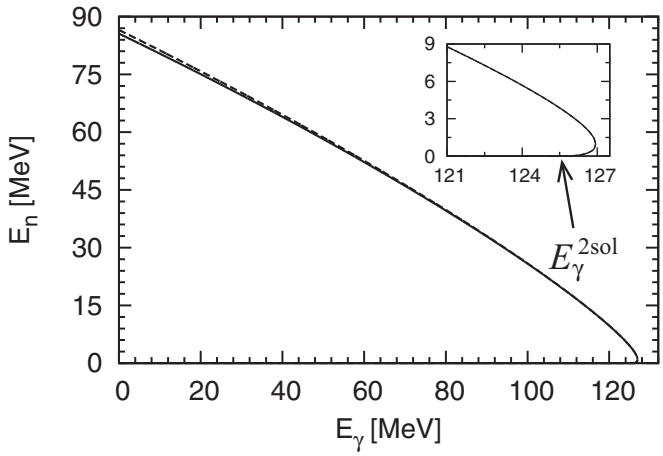

FIG. 10. The kinematically allowed region in the E_γ-E_n plane calculated relativistically (solid curve) and nonrelativistically (dashed curve) for the $\pi^- + {}^3\mathrm{H} \to \gamma + n + n + n$ capture process.

The values of the differential capture rates $d\Gamma_{nnn}/dE_\gamma$ are smaller (see Fig. 11) than the $d\Gamma_{nnp}/dE_\gamma$ results for the three-body breakup of ^{3}He. The maximum is still broader for the plane wave case but FSI now *raises* the results by a factor of 1.8, playing a crucial role also for this process. The inclusion of the 3N force leads to a reduction of the peak's height by about 15%. Also the total rates for pion capture on ^{3}H are displayed in Table II and described in the next section.

VII. COMPARISON WITH EARLIER THEORETICAL PREDICTIONS

A comparison with earlier theoretical predictions and experimental data is not simple for several reasons. Experimental work never actually aimed at obtaining total radiative capture rates. Very often measurements covered different reaction channels and tried to gather information about their relative probabilities. The famous Panofsky ratio for ^{3}He, studied in Refs. [55,56], is a very good example. Unfortunately, such ratios involve rates, which are not calculated by us in the present paper. Also we do not have experimental (unnormalized) photon energy spectra for the reactions of interest at our disposal.

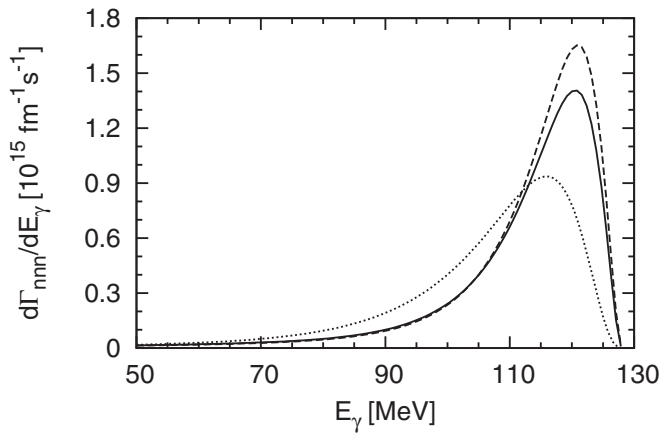

FIG. 11. The same as in the right panel of Fig. 8 but for the differential capture rate $d\Gamma_{nnn}/dE_\gamma$ in the case of the $\pi^- + {}^3\mathrm{H} \to \gamma + n + n + n$ process.

Many calculations for the $\pi^- + {}^2\mathrm{H} \to \gamma + n + n$ concentrated on the extraction of the nn scattering length and their authors did not provide results for the total radiative capture Γ_{nn}. This is because already Gibbs, Gibson, and Stephenson pointed out in Ref. [17] that the total radiative rate is clearly insensitive to uncertainties of the low-energy nn scattering parameters. Namely, they observed that variation of a_{nn} from -15 to -20 fm or the effective range r_{nn} from 2.6 to 3.0 fm changed Γ_{nn} by less than 1%. Thus predictions for the Γ_{nn} capture rate can be found in only few theoretical papers [17,76,77].

Additional problems are caused by the fact that some predictions originate from combined theoretical and experimental evidence. Finally, earlier calculations are often corrected in subsequent publications. Nonetheless, we have tried to collect the available information and we show it in Tables I and II.

In Table I the total radiative capture rates for the $\pi^- + {}^2\mathrm{H} \to \gamma + n + n$ reaction are displayed. As already mentioned, for this observable our plane wave and full results are rather similar despite the fact that final state rescattering is very important and substantially affects the differential rates in Figs. 2 and 3. We notice also that our full predictions agree with the earlier theoretical results, except for Ref. [17].

Table II contains rates for radiative capture in the trinucleons. We consider several capture channels, starting from the only nonbreakup process: $\pi^- + {}^3\mathrm{He} \to \gamma + {}^3\mathrm{H}$. Here the values of the rates are much higher than for the $\pi^- + {}^2\mathrm{H} \to \gamma + n + n$ reaction. The capture rate is raised by approximately 3.5%, when the 3N bound states are calculated consistently not only with the 2N but also with the 3N potentials.

The breakup of ^{3}He is clearly dominated by the $\pi^- + {}^3\mathrm{He} \to \gamma + n + d$ reaction, since the rate for the $\pi^- + {}^3\mathrm{He} \to \gamma + n + n + p$ process is three times smaller. For both breakup reactions FSI effects based on the 2N forces are very strong and reduce the rates significantly. The inclusion of the 3N force leads to a further reduction, which amounts to 9% (two-body breakup) and to 7% (three-body breakup). Our best results (obtained with the 3N force) for the ratio of the total breakup rate to the nonbreakup rate agree both with the experimental data from Ref. [57] and with the theoretical prediction in Ref. [55]. That means that the nonbreakup and breakup channels in radiative pion capture in ^{3}He are equally important.

Comparing the total rates for the $\pi^- + {}^3\mathrm{H} \to \gamma + n + n + n$ reaction, one might draw a false conclusion that FSI and 3N force effects are very small. From Fig. 11 it is, however, clear that the agreement between the plane wave and full results for the total rates is rather accidental, since the differential rates are quite different. Contrary to the three-body breakup of ^{3}He, FSI effects enhance the plane wave result. The 3N force reduces the rate by approximately 10%. Our result for the total radiative capture rate is by about 70% larger than the prediction from Ref. [62].

In view of the fact that the theoretical results obtained before were based on quite different approaches, in many

cases the agreement with earlier theoretical predictions is satisfactory. In particular, we obtained similar shapes of the photon energy spectra for all studied reactions. Our predictions about the role of the final state interactions based on the realistic semiphenomenological nuclear forces are fully converged with respect to the number of partial wave states. That means that, in contrast to Phillips and Roig [55,64], we are ready to calculate not only capture rates but also any polarization observables. Our much more advanced model confirms qualitatively the S-wave based results for capture rates from Refs. [55,64]. Thus it will be very interesting to compare results of modern calculations performed with improved transition operator and consistent nuclear forces.

VIII. SUMMARY AND CONCLUSIONS

Recent theoretical work by Gårdestig and Phillips [21,45] shows that radiative pion capture is not only interesting by itself but also correlated with a variety of other processes when studied within chiral effective field theory. This is very important because the other reactions (like muon capture) or neutrino induced processes are much harder to measure, and the information from the radiative capture on light nuclei could significantly improve our understanding of the other processes. Thus a uniform framework for the calculations of various electromagnetic and weak reactions on the single nucleon, deuteron, ^{3}He, ^{3}H, and other light nuclei should be formulated and applied. This framework would comprise consistent two-nucleon and more-nucleon forces as well as transition operators ("currents") with one-body and many-body parts. Results of fully converged calculations should be ultimately compared with precise experimental data, to yield a broad and complete picture of these reactions in few-nucleon systems.

In the present paper, we studied the $\pi^- + {}^2\mathrm{H} \to \gamma + n + n$, $\pi^- + {}^3\mathrm{He} \to \gamma + {}^3\mathrm{H}$, $\pi^- + {}^3\mathrm{He} \to \gamma + n + d$, $\pi^- + {}^3\mathrm{He} \to \gamma + n + n + p$, and $\pi^- + {}^3\mathrm{H} \to \gamma + n + n + n$ reactions using traditional nuclear forces (the AV18 NN potential and the Urbana IX 3N force) and a simple single-nucleon transition operator. These calculations, like our studies of muon capture [65,66] or very recent investigations of some neutrino induced reactions [78], are ready to be systematically improved to encompass more complicated dynamical input. Many aspects of the performed calculations—like the role of the relativistic kinematics, the efficient methods of partial wave decomposition, or the convergence of our results with respect to the number of partial wave states—have been established already, and the predictions presented here can serve as an important benchmark.

Our calculations already provide first realistic predictions for the differential $d\Gamma_{^3\mathrm{H}}/dE_\gamma$, $d\Gamma_{nd}/dE_\gamma$, $d\Gamma_{nnp}/dE_\gamma$, and $d\Gamma_{nnn}/dE_\gamma$ capture rates as well as for the corresponding total radiative capture rates $\Gamma_{^3\mathrm{H}}$, Γ_{nd}, Γ_{nnp}, and Γ_{nnn}. The formalism used in the present paper will be extended in the future to study other pion capture reactions, including nonradiative and double radiative pion capture.

ACKNOWLEDGMENTS

We would like to thank Peter Truöl for drawing our attention to radiative pion capture and for providing us with crucial references. This work is a part of the LENPIC project and was supported by the Polish National Science Centre under Grants No. 2016/22/M/ST2/00173 and No. 2016/21/D/ST2/01120 and by DFG and NSFC through funds provided to the Sino-German CRC 110 "Symmetries and the Emergence of Structure in QCD" [NSFC (11621131001), DFG (TRR110)]. The numerical calculations were partially performed on the supercomputer cluster of the JSC, Jülich, Germany.

APPENDIX A: THE 2N MATRIX ELEMENTS

For the $\pi^- + {}^2\mathrm{H} \to \gamma + n + n$ reaction the nuclear matrix element $N_{nn,\pm1}(m_1, m_2, m_d)$ introduced in Eq. (3.3) is evaluated as

$$N_{nn,\pm1}(m_1, m_2, m_d) \equiv {}^{(-)}\langle \mathbf{p} m_1 m_2 \mid j_{A,\pm1} \mid \phi_d m_d \rangle, \quad \text{(A1)}$$

where $\mid \phi_d m_d \rangle$ is the initial deuteron state with the spin projection m_d and $\mid \mathbf{p} m_1 m_2 \rangle^{(-)}$ is the antisymmetrized two-neutron scattering state with the relative momentum $\mathbf{p}$ and the individual neutron spin projections m_1 and m_2. While the deuteron state is obtained in momentum space as a solution to a simple algebraic eigenvalue problem,

$$\left(H_0^{2N} + V\right) \mid \phi_d \rangle = E_d \mid \phi_d \rangle, \quad \text{(A2)}$$

where H_0^{2N} is the free 2N Hamiltonian and V is a given NN potential, the 2N scattering state is formally defined as

$$\mid \mathbf{p} m_1 m_2 \rangle^{(-)} \equiv \lim_{\epsilon \to 0^+} \frac{-i\epsilon}{E_{2N} - i\epsilon - H_0^{2N} - V} \mid \mathbf{p} m_1 m_2 \rangle \quad \text{(A3)}$$

and can be readily computed from the scattering t matrix as

$$|\mathbf{p} m_1 m_2\rangle^{(-)} = \lim_{\epsilon \to 0^+} \left(1 + G_0^{2N}(E_{2N} - i\epsilon) t (E_{2N} - i\epsilon)\right) |\mathbf{p} m_1 m_2\rangle, \quad \text{(A4)}$$

where $G_0^{2N}(E_{2N})$ is the free 2N propagator, and the kinetic energy of the relative motion in the 2N system, $E_{2N} = \frac{\mathbf{p}^2}{M}$, is given by the energy-momentum conservation, which for the pionic atom at rest in our nonrelativistic approximation reads

$$M_{\pi^-} + M_d = \mid \mathbf{p}_\gamma \mid + 2M_n + \frac{\mathbf{p}_\gamma^2}{4M_n} + \frac{\mathbf{p}^2}{M_n}, \quad \text{(A5)}$$

where M_{π^-}, M_d, M_n, $\mathbf{p}_\gamma$ are the negative pion mass, deuteron mass, neutron mass, and the final photon momentum, respectively. Finally, the t matrix is obtained as a solution of the Lippmann-Schwinger equation:

$$t(E_{2N}) = V + t(E_{2N}) G_0^{2N}(E_{2N}) V. \quad \text{(A6)}$$

Using Eq. (A4), the nuclear matrix element (A1) becomes

$$N_{nn,\pm1}(m_1, m_2, m_d) = \langle \mathbf{p} m_1 m_2 | \left(1 + t(E_{2N}) G_0^{2N}(E_{2N})\right) j_{A,\pm1}(\mathbf{P}_f, \mathbf{P}_i) | \phi_d m_d \rangle, \quad \text{(A7)}$$

with $\mathbf{P}_i = 0$ and $\mathbf{P}_f = -\mathbf{p}_\gamma$.

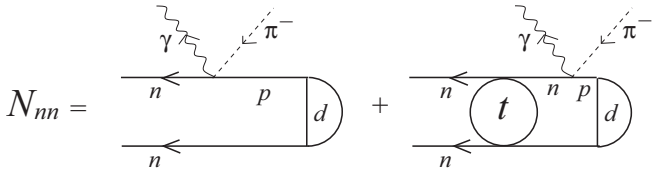

FIG. 12. Diagrammatic representation of the 2N matrix element for the radiative pion capture reaction, assuming a single-nucleon mechanism. The circular segment on the right stands for the initial deuteron. The left diagram corresponds to the plane wave (PW) part of $N_{nn,\pm1}$, and the circle in the second diagram represents the rescattering described by the t matrix.

The sense of this equation can be explained diagrammatically, as shown in Fig. 12, where we assumed that the negative pion is absorbed only by the single proton. Namely the nuclear matrix element contains the plane wave (PW) part and the rescattering term, with the t matrix present.

APPENDIX B: THE 3N MATRIX ELEMENTS

In the general case the 3N Hamiltonian H contains the 3N kinetic energy (H_0), potential energies for each two-body subsystem (V_{12}, V_{23}, and V_{31}), as well as the three-body potential energy (V_{123}), usually called a 3N force (3NF). It is always possible to decompose V_{123} into three terms,

$$V_{123} = V^{(1)} + V^{(2)} + V^{(3)}, \tag{B1}$$

in such a way that $V^{(i)}$ is symmetric under the exchange of nucleons j and k ($i, j, k = 1, 2, 3, i \neq j \neq k \neq i$).

We calculate the 3N bound states in the Faddeev scheme, using the method described, for example, in Ref. [79]. First we solve the Faddeev equation

$$|\,\psi\rangle = G_0 t_{23} P\,|\,\psi\rangle + (1 + G_0 t_{23}) G_0 V^{(1)}(1 + P)\,|\,\psi\rangle, \tag{B2}$$

where $|\,\psi\rangle$ is the Faddeev component of the full 3N wave function $|\,\Psi\rangle$, $G_0 \equiv 1/(E - H_0)$ is the free 3N propagator, t_{23} is the two-body t operator for the (2,3) subsystem, and $P \equiv P_{12}P_{23} + P_{13}P_{23}$ is the permutation operator built from transpositions P_{ij}, which interchange nucleons i and j. The wave function $|\,\Psi\rangle$ is easily obtained from the Faddeev component as

$$|\,\Psi\rangle = (1 + P)\,|\,\psi\rangle. \tag{B3}$$

We distinguish between the strong neutron-neutron and proton-proton forces, obtaining the ^{3}He and ^{3}H wave functions and in the latter case include also the Coulomb potential acting between the two protons.

Although many-nucleon mechanisms of pion radiative capture are neglected in the present work, the 3N current operator j^μ_{3N} might in principle contain the single-nucleon, 2N, and 3N contribution. Therefore we write (μ denotes any component of the current operator):

$$j^\mu_{3N} = j^\mu_1 + j^\mu_2 + j^\mu_3 + j^\mu_{12} + j^\mu_{23} + j^\mu_{31} + j^\mu_{123}, \tag{B4}$$

where the 3N part can be split into three parts (just like the 3NF), $j^\mu_{123} = j^{\mu 1} + j^{\mu 2} + j^{\mu 3}$. Thus we can decompose the 3N current operator into three parts, $j^\mu(i)$ ($i = 1, 2, 3$), which

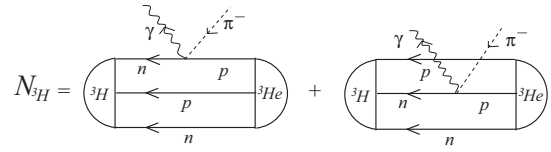

FIG. 13. Diagrammatic representation of the 3N matrix element for the $\pi^- + {}^3\mathrm{He} \to \gamma + {}^3\mathrm{H}$ reaction, assuming that the pion is captured only by single protons. The circular segment on the right (left) stands for initial ^{3}He (final ^{3}H).

possess the same symmetry properties as $V^{(i)}$:

$$j^\mu_{3N} = j^\mu(1) + j^\mu(2) + j^\mu(3), \tag{B5}$$

where for example $j^\mu(1) \equiv j^\mu_1 + j^\mu_{23} + j^{\mu 1}$. As in the 2N case, we have to consider only two spherical components of the current operator, j_{+1} and j_{-1}.

For a given choice of the 3N Hamiltonian and the current operator, the nuclear matrix elements $N_{\pm1}(m_{^3\mathrm{H}}, m_{^3\mathrm{He}})$ are calculated as given in Eq. (4.7). Figure 13 corresponds to a particular case where radiative pion capture in ^{3}He can take place only on two individual protons inside the nucleus.

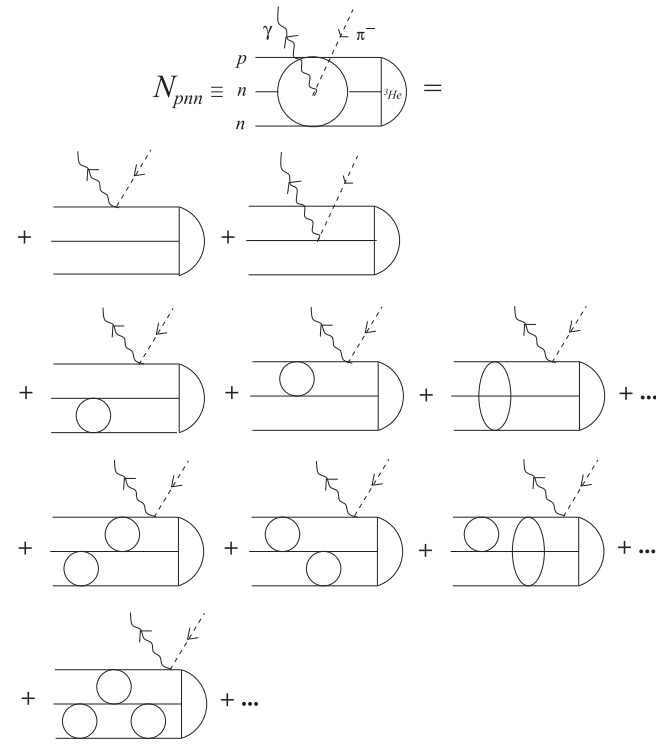

FIG. 14. The same as in Fig. 13 but for the $\pi^- + {}^3\mathrm{He} \to \gamma + p + n + n$ breakup reaction, assuming a single-nucleon pion capture mechanism and neglecting the 3N force. The open circles and ovals represent the two-nucleon t matrices acting in the three different subsystems. The subsequent rows show the symmetrized plane wave contributions (SPW) and selected diagrams representing rescattering of the first, second, and third order in the t matrix.

The matrix elements for the nucleon-deuteron (Nd) channel

$$N^{\mu}_{Nd} = \langle \Psi^{(-)}_{Nd} \mid j^{\mu}_{3N} \mid \Psi \rangle \tag{B6}$$

and the 3N breakup channel

$$N^{\mu}_{3N} = \langle \Psi^{(-)}_{3N} \mid j^{\mu}_{3N} \mid \Psi \rangle \tag{B7}$$

comprise the corresponding channel scattering states. Actually we do not compute these 3N scattering states explicitly, but solve a Faddeev-type equation for an auxiliary state $\mid U^{\mu} \rangle$ [74],

$$\begin{aligned} \mid U^{\mu} \rangle = & \left(t_{23} G_0 + \frac{1}{2}(1+P) V^{(1)} G_0 (1 + t_{23} G_0) \right) \\ & \times (1+P) j^{\mu}(1) \mid \Psi \rangle + \Big(t_{23} G_0 P \\ & + \frac{1}{2}(1+P) V^{(1)} G_0 (1 + t_{23} G_0) P \Big) \mid U^{\mu} \rangle. \end{aligned} \tag{B8}$$

The solutions of Eq. (B8) are calculated for each component of the current operator and two kinematical quantities: the 3N internal energy $E_{c.m.}$ and the magnitude of the three-momentum transferred to the 3N system, $\mid \mathbf{Q} \mid$. It is, however, crucial that $\mid U^{\mu} \rangle$ is independent of the final state kinematics.

The matrix elements N^{μ}_{Nd} and N^{μ}_{3N} for arbitrary exclusive kinematics are then generated by simple quadratures:

$$N^{\mu}_{Nd} = \langle \phi_{Nd} \mid (1+P) j^{\mu}(1) \mid \Psi \rangle + \langle \phi_{Nd} \mid P \mid U^{\mu} \rangle, \tag{B9}$$

$$\begin{aligned} N^{\mu}_{3N} = & \langle \phi_{3N} \mid (1+P) j^{\mu}(1) \mid \Psi \rangle \\ & + \langle \phi_{3N} \mid t_{23} G_0 (1+P) j^{\mu}(1) \mid \Psi \rangle \\ & + \langle \phi_{3N} \mid P \mid U^{\mu} \rangle + \langle \phi_{3N} \mid t_{23} G_0 P \mid U^{\mu} \rangle, \end{aligned} \tag{B10}$$

where $\mid \phi_{Nd} \rangle$ is a product of the internal deuteron state and the state describing the free relative motion of the third nucleon with respect to the deuteron, and $\mid \phi_{3N} \rangle$ is a state [antisymmetrized in the (2,3) subsystem] representing the free motion of the three outgoing nucleons. Note that for the two breakup channels the SPW approximations are obtained with $N^{\mu}_{Nd,SPW} = \langle \phi_{Nd} \mid (1+P) j^{\mu}(1) \mid \Psi \rangle$ and $N^{\mu}_{3N,SPW} = \langle \phi_{3N} \mid (1+P) j^{\mu}(1) \mid \Psi \rangle$, respectively.

Exclusive observables can be further integrated over suitable phase space domains to obtain the semiexclusive or fully inclusive observables. The 3N Faddeev-type equation (B8) is solved by iterations in the partial wave momentum-space basis [74]. In order to achieve convergence, the calculations employ all partial wave states with the total 2N subsystem angular momentum $j \leqslant 4$ and the total 3N angular momentum $J \leqslant 15/2$.

In Fig. 14 the physical contents of the nuclear matrix element for one of the breakup channels is shown diagrammatically. For the case of the $\pi^- + {}^3\mathrm{He} \rightarrow \gamma + p + n + n$ process we show various contributions stemming from the SPW approximation and rescattering in different orders of the t matrix. A similar diagram can be drawn for the two-body breakup reaction.

[1] W. K. H. Panofsky, R. Lee Aamodt, and J. Hadley, Phys. Rev. **81**, 565 (1951).
[2] H. W. Baer, K. M. Crowe, and P. Truöl, Adv. Nucl. Phys. **9**, 177 (1977).
[3] D. Renker, W. Dahme, W. Hering, H. Panke, Č. Zupančič, J. C. Alder, B. Gabioud, C. Joseph, J. F. Loude, N. Morel, J. P. Perroud, A. Perrenoud, M. T. Tran, E. Winkelmann, G. Strassner, and P. Truöl, Phys. Rev. Lett. **41**, 1279 (1978).
[4] G. W. Reynaud and F. Tabakin, Phys. Rev. C **23**, 2652 (1981).
[5] C. J. Martoff, J. A. Bistirlich, C. W. Clawson, K. M. Crowe, M. Koike, J. P. Miller, S. S. Rosenblum, W. A. Zajc, H. W. Baer, A. H. Wapstra, G. Strassner, and P. Truöl, Phys. Rev. C **27**, 1621 (1983).
[6] Helmut W. Baer, J. A. Bistirlich, K. M. Crowe, W. Dahme, C. Joseph, J. P. Perroud, M. Lebrun, C. J. Martoff, U. Straumann, and P. Truöl, Phys. Rev. C **28**, 761 (1983).
[7] F. Roig and J. Navarro, Nucl. Phys. A **440**, 659 (1985).
[8] M. K. Singham and F. Tabakin, Phys. Rev. C **34**, 637 (1986).
[9] H. Krivine, E. Lipparini, J. Navarro, and F. Roig, Nucl. Phys. A **481**, 781 (1988).
[10] J. Navarro and F. Roig, Phys. Rev. C **39**, 302 (1989).
[11] K. J. Raywood, J. B. Lange, G. Jones, M. Pavan, M. E. Sevior, D. A. Hutcheon, A. Olin, D. Ottewell, S. Yen, S. J. Lee, K. S. Sim, A. Altman, E. Friedman, and A. Trudel, Phys. Rev. C **55**, 2492 (1997).
[12] J. E. Amaro, A. M. Lallena, and J. Nieves, Nucl. Phys. A **623**, 529 (1997).
[13] K. M. Watson and R. N. Stuart, Phys. Rev. **82**, 738 (1951).
[14] K. McVoy, Phys. Rev. **121**, 1401 (1961).
[15] M. Bander, Phys. Rev. **134**, B1052 (1964).
[16] W. R. Gibbs, B. F. Gibson, and G. J. Stephenson, Jr., Phys. Rev. C **11**, 90 (1975); **12**, 2130(E) (1975).
[17] W. R. Gibbs, B. F. Gibson, and G. J. Stephenson, Jr., Phys. Rev. C **16**, 327 (1977); **17**, 856(E) (1978).
[18] G. F. de Téramond, Phys. Rev. C **16**, 1976 (1977).
[19] G. F. de Téramond and B. Gabioud, Phys. Rev. C **36**, 691 (1987).
[20] A. Gårdestig and D. R. Phillips, Phys. Rev. C **73**, 014002 (2006).
[21] A. Gårdestig and D. R. Phillips, Phys. Rev. Lett. **96**, 232301 (2006).
[22] R. H. Phillips and K. M. Crowe, Phys. Rev. **96**, 484 (1954).
[23] J. W. Ryan, Phys. Rev. Lett. **12**, 564 (1964).
[24] P. Haddock, R. M. Salter, Jr., M. Zeller, J. B. Czirr, and D. R. Nygren, Phys. Rev. Lett. **14**, 318 (1965).
[25] J. P. Nicholson, P. G. Butler, N. Cohen, and A. N. James, Phys. Lett. B **27**, 452 (1968).
[26] R. M. Salter, Jr., R. P. Haddock, M. Zeller, D. R. Nygren, and J. B. Czirr, Nucl. Phys. A **254**, 241 (1975).
[27] B. Gabioud, J.-C. Alder, C. Joseph, J.-F. Loude, N. Morel, A. Perrenoud, J.-P. Perroud, M. T. Tran, E. Winkelmann, W. Dahme, H. Panke, D. Renker, Č. Zupančič, G. Strassner, and P. Truöl, Phys. Rev. Lett. **42**, 1508 (1979).
[28] B. Gabioud *et al.*, Phys. Lett. B **103**, 9 (1981).

[29] B. Gabioud *et al.*, Nucl. Phys. A **420**, 496 (1984).
[30] O. Schori, B. Gabioud, C. Joseph, J. P. Perroud, D. Rüegger, M. T. Tran, P. Truöl, E. Winkelmann, and W. Dahme, Phys. Rev. C **35**, 2252 (1987).
[31] C. R. Howell *et al.*, Phys. Lett. B **444**, 252 (1998).
[32] Q. Chen, C. R. Howell, T. S. Carman, W. R. Gibbs, B. F. Gibson, A. Hussein, M. R. Kiser, G. Mertens, C. F. Moore, C. Morris, A. Obst, E. Pasyuk, C. D. Roper, F. Salinas, H. R. Setze, I. Slaus, S. Sterbenz, W. Tornow, R. L. Walter, C. R. Whiteley, and M. Whitton, Phys. Rev. C **77**, 054002 (2008).
[33] I. Slaus, Y. Akaishi, and H. Tanaka, Phys. Rep. **173**, 257 (1989).
[34] A. Gårdestig, J. Phys. G **36**, 053001 (2009).
[35] V. Huhn, L. Wätzold, Ch. Weber, A. Siepe, W. von Witsch, H. Witała, and W. Glöckle, Phys. Rev. Lett. **85**, 1190 (2000).
[36] D. E. Gonzalez Trotter *et al.*, Phys. Rev. C **73**, 034001 (2006).
[37] W. R. Gibbs, B. F. Gibson, and G. J. Stephenson, Jr., Phys. Rev. C **16**, 322 (1977).
[38] R. V. Reid, Ann. Phys. **50**, 411 (1968).
[39] N. I. Muskhelishvili, *Singular Integral Equations* (Noordhoff, Groningen, Netherlands, 1953).
[40] R. Omnès, Nuovo Cimento **8**, 316 (1958); M. Jacob, G. Mahoux, and R. Omnès, *ibid.* **23**, 838 (1962).
[41] G. F. de Téramond, J. Páez, and C. W. Soto Vargas, Phys. Rev. C **21**, 2542 (1980).
[42] V. Bernard, N. Kaiser, and U.-G. Meißner, Z. Phys. C **70**, 483 (1996).
[43] V. Bernard, N. Kaiser, and U.-G. Meißner, Phys. Lett. B **383**, 116 (1996).
[44] H. W. Fearing, T. R. Hemmert, R. Lewis, and Ch. Unkmeir, Phys. Rev. C **62**, 054006 (2000).
[45] A. Gårdestig, Phys. Rev. C **74**, 017001 (2006).
[46] A. M. L. Messiah, Phys. Rev. **87**, 639 (1952).
[47] N. M. Kroll and M. A. Ruderman, Phys. Rev. **93**, 233 (1954).
[48] P. P. Divakaran, Phys. Rev. **139**, B387 (1965).
[49] M. Ericson and A. Figureau, Nucl. Phys. B **3**, 609 (1967).
[50] M. Ericson and A. Figureau, Nucl. Phys. B **11**, 621 (1969).
[51] D. Griffiths and C. Kim, Phys. Rev. **173**, 1584 (1968).
[52] P. Pascual and A. Fujii, Nuovo Cimento **65**, 411 (1970).
[53] O. A. Zaimidoroga *et al.*, J. Exptl. Theoret. Phys. (U.S.S.R.) **48**, 1267 (1965) [Sov. Phys. JETP **21**, 848 (1965)].
[54] O. A. Zaimidoroga *et al.*, J. Exptl. Theoret. Phys. (U.S.S.R.) **51**, 1646 (1966) [Sov. Phys. JETP **24**, 1111 (1967)].
[55] A. C. Phillips and F. Roig, Nucl. Phys. A **234**, 378 (1974).
[56] W. R. Gibbs, B. F. Gibson, and G. J. Stephenson, Jr., Phys. Rev. C **18**, 1761 (1978).
[57] P. Truöl, H. W. Baer, J. A. Bistirlich, K. M. Crowe, N. de Botton, and J. A. Helland, Phys. Rev. Lett. **32**, 1268 (1974).
[58] A. Fuji and D. J. Hall, Nucl. Phys. **32**, 102 (1962).
[59] J. Delorme and T. E. O. Ericson, Phys. Lett. **21**, 98 (1966).
[60] R. D. Amado, Phys. Rev. **132**, 485 (1963).
[61] C. Lovelace, Phys. Rev. **135**, B1225 (1964).
[62] A. C. Phillips and F. Roig, in *High Energy Physics and Nuclear Structure*, edited by D. E. Nagle *et al.*, AIP Conference Proceedings No. 26 (American Institute of Physics, New York, 1975).
[63] J. A. Bistirlich *et al.*, Phys. Rev. Lett. **36**, 942 (1976).
[64] J. P. Miller *et al.*, Nucl. Phys. A **343**, 341 (1980).
[65] J. Golak, R. Skibiński, H. Witała, K. Topolnicki, A. E. Elmeshneb, H. Kamada, A. Nogga, and L. E. Marcucci, Phys. Rev. C **90**, 024001 (2014).
[66] J. Golak, R. Skibiński, H. Witała, K. Topolnicki, H. Kamada, A. Nogga, and L. E. Marcucci, Phys. Rev. C **94**, 034002 (2016).
[67] L. E. Marcucci, M. Piarulli, M. Viviani, L. Girlanda, A. Kievsky, S. Rosati, and R. Schiavilla, Phys. Rev. C **83**, 014002 (2011).
[68] A. Kievsky, S. Rosati, M. Viviani, L. E. Marcucci, and L. Girlanda, J. Phys. G **35**, 063101 (2008).
[69] G. Shen, L. E. Marcucci, J. Carlson, S. Gandolfi, and R. Schiavilla, Phys. Rev. C **86**, 035503 (2012).
[70] R. B. Wiringa, V. G. J. Stoks, and R. Schiavilla, Phys. Rev. C **51**, 38 (1995).
[71] B. S. Pudliner, V. R. Pandharipande, J. Carlson, Steven C. Pieper, and R. B. Wiringa, Phys. Rev. C **56**, 1720 (1997).
[72] K. Topolnicki, J. Golak, R. Skibiński, A. E. Elmeshneb, W. Glöckle, A. Nogga, and H. Kamada, Few-Body Syst. **54**, 2223 (2013).
[73] J. D. Walecka, *Theoretical Nuclear and Subnuclear Physics* (Oxford University Press, New York, 1995).
[74] J. Golak, R. Skibiński, H. Witała, W. Glöckle, A. Nogga, and H. Kamada, Phys. Rep. **415**, 89 (2005).
[75] R. Skibiński, J. Golak, H. Witała, W. Glöckle, and A. Nogga, Eur. Phys. J. A **24**, 11 (2005).
[76] A. Reitan, Nucl. Phys. **87**, 232 (1966).
[77] M. Sotona and E. Truhlik, Nucl. Phys. A **262**, 400 (1976).
[78] J. Golak, R. Skibiński, K. Topolnicki, H. Witała, A. Grassi, H. Kamada, and L. E. Marcucci, Phys. Rev. C **98**, 015501 (2018).
[79] A. Nogga, D. Hüber, H. Kamada, and W. Glöckle, Phys. Lett B **409**, 19 (1997).